



HAL
open science

Low-Altitude Observations of Recurrent Short-Lived keV Ion Micro-Injections Inside the Diffuse Auroral Zone

J.-A. Sauvaud, Dominique C. Delcourt, Michel Parrot, D. Payan, T. Raita, E. Penou

► **To cite this version:**

J.-A. Sauvaud, Dominique C. Delcourt, Michel Parrot, D. Payan, T. Raita, et al.. Low-Altitude Observations of Recurrent Short-Lived keV Ion Micro-Injections Inside the Diffuse Auroral Zone. Journal of Geophysical Research Space Physics, 2018, 123, pp.2054-2063. 10.1002/2017JA025075 . insu-01744917

HAL Id: insu-01744917

<https://insu.hal.science/insu-01744917>

Submitted on 25 Oct 2018

HAL is a multi-disciplinary open access archive for the deposit and dissemination of scientific research documents, whether they are published or not. The documents may come from teaching and research institutions in France or abroad, or from public or private research centers.

L'archive ouverte pluridisciplinaire **HAL**, est destinée au dépôt et à la diffusion de documents scientifiques de niveau recherche, publiés ou non, émanant des établissements d'enseignement et de recherche français ou étrangers, des laboratoires publics ou privés.



RESEARCH ARTICLE

10.1002/2017JA025075

Key Points:

- We present new ion structures in the diffuse auroral zone during storm recovery phase
- Recurrent dispersion features in the keV range are shown to be due to time-of-flight effects
- The microinjections result from impulsive ion diffusion in the 8,000–12,000 km altitudinal range

Correspondence to:

J.-A. Sauvaud,
jsauvaud@irap.omp.eu

Citation:

Sauvaud, J.-A., Delcourt, D., Parrot, M., Payan, D., Raita, T., & Penou, E. (2018). Low-altitude observations of recurrent short-lived keV ion microinjections inside the diffuse auroral zone. *Journal of Geophysical Research: Space Physics*, 123, 2054–2063. <https://doi.org/10.1002/2017JA025075>

Received 30 NOV 2017

Accepted 16 MAR 2018

Accepted article online 23 MAR 2018

Published online 30 MAR 2018

©2018. The Authors.

This is an open access article under the terms of the Creative Commons Attribution-NonCommercial-NoDerivs License, which permits use and distribution in any medium, provided the original work is properly cited, the use is non-commercial and no modifications or adaptations are made.

Low-Altitude Observations of Recurrent Short-Lived keV Ion Microinjections Inside the Diffuse Auroral Zone

J.-A. Sauvaud¹ , D. Delcourt^{2,3} , M. Parrot³ , D. Payan⁴, T. Raita⁵ , and E. Penou¹

¹Institut de Recherche en Astrophysique et Planétologie, Université de Toulouse, CNRS, UPS, CNES, Toulouse, France,

²Laboratoire de Physique des Plasmas, Ecole Polytechnique, CNRS, Université Pierre et Marie Curie, Palaiseau, France,

³Laboratoire de Physique et Chimie de l'Environnement et de l'Espace, CNRS, Université d'Orléans, Orléans, France, ⁴Centre National d'Etudes Spatiales, Toulouse, France, ⁵Sodankylä Geophysical Observatory, University of Oulu, Sodankylä, Finland

Abstract The AMBRE experiment onboard the ocean topography mapper JASON-3 aims at measuring the spacecraft potential as well as auroral particle precipitation using two top-hat analyzers for electrons and ions in the 20 eV–28 keV energy range. The JASON-3 spacecraft has a nearly circular orbit at an altitude of 1,336 km with an inclination of 66°, at times probing the equatorward part of the auroral oval in a nearly tangential manner upon leaving the outer radiation belt. In this region of space, during periods of enhanced geomagnetic activity with small or moderate storms, AMBRE detected recurrent “microinjections” of ions with energies in the 200 eV–28 keV range and which exhibit clear time-of-flight dispersion. Ray tracing using single trajectory computations suggests that these ions are launched from a source located in the 8,000–12,000 km altitudinal range and subsequently propagate downward toward the ionosphere. Such observations of quasiperiodic dispersed downflowing ions are new, and we argue that these structures could be produced by ion-wave interactions at midaltitudes.

1. Introduction

Dispersed ion structures in the auroral zone have been reported in a number of observational studies. Some key features may be extracted from these studies, most dispersions being interpreted as the result of either the effect of the large-scale convection electric field or time-of-flight effects acting on particles ejected from the equatorial vicinity. For example, in the cusp region near noon, the convection electric field transports low-energy ions toward high latitudes when the interplanetary magnetic field points southward, which leads to clear energy-latitude dispersion (e.g., Reiff et al., 1977; Rosenbauer, 1975; Shelley et al., 1976; Smith & Lockwood, 1996). Sporadic and recurrent ion injections originating from the low-latitude boundary layers have also been reported by Woch and Lundin (1992) and Stenuit et al. (2001) in the dawn and dusk sectors of the auroral oval.

In the nightside sector, time-of-flight effects have been invoked to explain repetitive dispersed ion structures measured near the poleward boundary of the auroral oval during substorms, the source regions being located in the nightside close to the equatorial plane (Sauvaud et al., 1999; Sergeev et al., 2000). These ions subsequently drift in longitude, while bouncing between mirror points, which leads to further energy dispersed structures (Hirahara et al., 1996, 1997). In the low-latitude dayside sector, multiple bands of ions have been observed near the equatorial edge of the auroral zone by the DE 1 and DE 2 spacecraft (Frahm et al., 1986; Winningham et al., 1984). Here it was proposed that the decreasing ion energy with decreasing latitude was due to convective dispersion. More recent FAST observations of multi-energy events near local noon at several thousand kilometers altitude were proposed to have originated in a temporally localized, spatially extended, equatorial source (Boehm et al., 1999).

In the inner nightside magnetosphere, Mauk (1986) argued that some dispersed ion structures during substorms may follow from impulsive energization and related breaking of the second adiabatic invariant due to the short-lived electric field induced by magnetic field line reconfigurations. Close to the plasmopause inside the diffuse aurora, the convection and corotation electric fields are at the root of energy structures for ions of both magnetospheric and ionospheric origins. For example, Delcourt et al. (1999) showed how low-energy ions extracted from auroral arcs in the high-latitude ionosphere can be transported to lower latitudes and locally form a sub-keV population. In the morning side of the diffuse auroral zone, low-energy ion bands are systematically detected and are presumed to be generated by drifting under the combined effect of magnetic and electric fields after substorms (e.g., Hirahara et al., 1997; Kovrazhkin et al., 1999; Sauvaud

et al., 1981; Yamauchi et al., 2014). More recently, during the strongest geomagnetic storms encountered by FAST and DEMETER satellites, long-lasting energy-banded ions have been detected in the low-latitude subauroral zone over L values ranging from ~ 2 to 3.5, in conjunction with banded very low frequency emissions (Colpitts et al., 2012).

In this study, we report a new type of dispersive structures recorded in the 200 eV–28 keV energy range. These structures were observed near the equatorward boundary of the diffuse auroral zone in the midnight sector during episodes of small to moderate storms and enhanced electrojet currents. We will show that these structures result from time-of-flight dispersion of ions propagating downward from a source located not in the equatorial region but at altitudes of 1–2 Earth radii (R_E). We find that the microinjections are related to ultralow frequency (ULF) waves with quasi-periods on the order of 10 s as evidenced from pulsation magnetometers in the conjugate area of the satellite. We argue that the microinjections result from nonlinear interactions of keV ions with electromagnetic ion cyclotron waves (EMIC) modulated by the ULF waves.

2. Instrumentation

The measurements reported in this study were obtained from the AMBRE instrument onboard JASON-3, which is a three-axis stabilized spacecraft that was launched on 17 January 2016 on a nearly circular orbit at 1,336 km altitude and 66° inclination. AMBRE consists of two coupled top-hat analyzers, one for ions and the other for electrons in the 20 eV–28 keV energy range. The field of view of both spectrometers is $180^\circ \times 6^\circ$ centered on the zenith. The 180° plane of view is divided into four anodes, the two central ones (sectors 2 and 3) looking at precipitating particles while the two side ones (sectors 1 and 4) record nearly trapped particles (note that the angular resolution of each anode is only $\sim 35^\circ$). The geometries of both electron and ion analyzers are identical, except that the electron analyzer has an entrance grid with a transparency of 10% (Sauvaud & Payan, 2017). The AMBRE spectrometers provide particle spectra with 128, 32, or 16 energy steps with a time resolution that varies from 0.5 to 2 s. Most of the particle spectra presented in this study are with 16 energy steps acquired in 2 s. The geometrical factor of a single anode is $1.7 \cdot 10^{-3} \text{ cm}^2 \cdot \text{ster.eV/eV}$ for ions and $1.5 \cdot 10^{-4} \text{ cm}^2 \cdot \text{ster.eV/eV}$ for electrons.

3. Data Presentation

To set up the framework of this study, Figure 1 shows the Dst index for the AMBRE data periods of interest, indicated by red dotted vertical lines. It can be seen in Figure 1 that all the cases that will be discussed here occurred during the recovery phase of small or moderate storms. Figure 2 shows a typical example of banded ions observed by AMBRE during these passes. This figure shows measurements from 21:45:30 UT to 21:54:30 UT on 3 February 2017, which corresponds to a disturbed magnetic period within a small storm recovery phase (Dst = -22 nT in Figure 1). The spacecraft reaches its maximum invariant latitude over Scandinavia at this time, allowing us to use local auroral indices to further characterize the observational context. These indices include IL and IU values (and equivalent AL and AU, respectively) deduced from the IMAGE magnetometer chain. They are shown in Figure 3a, which reveals that the pass occurred during a period of strong IL index (≈ -400 nT) at the beginning of the recovery phase of successive substorms starting around 19:45 UT on the same day.

The top panel of Figure 2 displays the color-coded energy flux of electrons measured from 20 eV up to 28 keV over 180° , while the middle and bottom panels of this figure are for ions in the same energy range but for pitch angles of $55\text{--}90^\circ$ and $10\text{--}35^\circ$, respectively. Note that, during this pass, JASON-3 was located close to midnight. In Figure 2, banded ions are noticeable at invariant latitudes between 64° and 65.2° , which corresponds to an L range of 5.2 to 5.68. The AMBRE electron spectrometer also detected plasma sheet electrons around 10 keV and secondary low-energy electrons of ionospheric origin. Note that weak discrete arcs are embedded inside the diffuse auroral zone, which is a known characteristic of this aurora (e.g., Lui et al., 1977). In addition, note that at the beginning and at the end of the time interval in Figure 2, the satellite was inside the outer radiation belt, as evidenced from the nearly uniform background fluxes detected over the whole energy range.

Figure 2 shows a prominent correlation between the occurrence of trapped ion structures and the weak and discrete structures of auroral electrons at energies below ~ 200 eV. In particular, while dispersed ion bands are clearly noticeable in the energy spectrogram of nearly trapped ions (center panel), these bands are much less

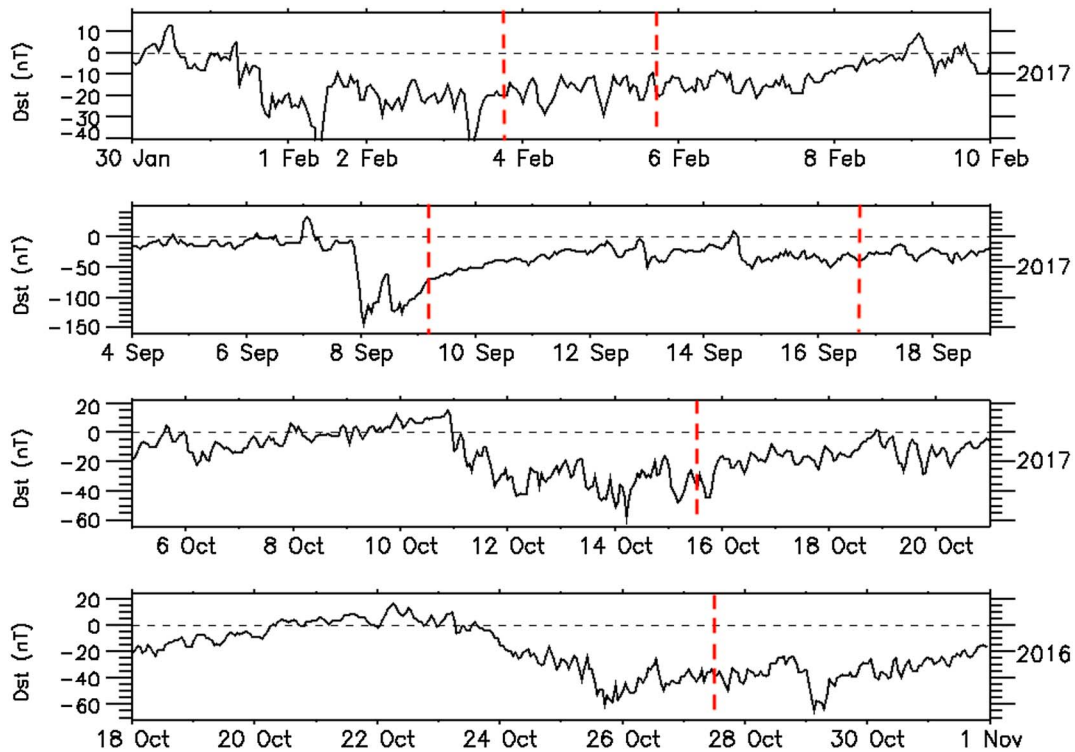


Figure 1. Dst indices for the six JASON-3 passes presented in this study. The dashed red lines indicate the times of the passes.

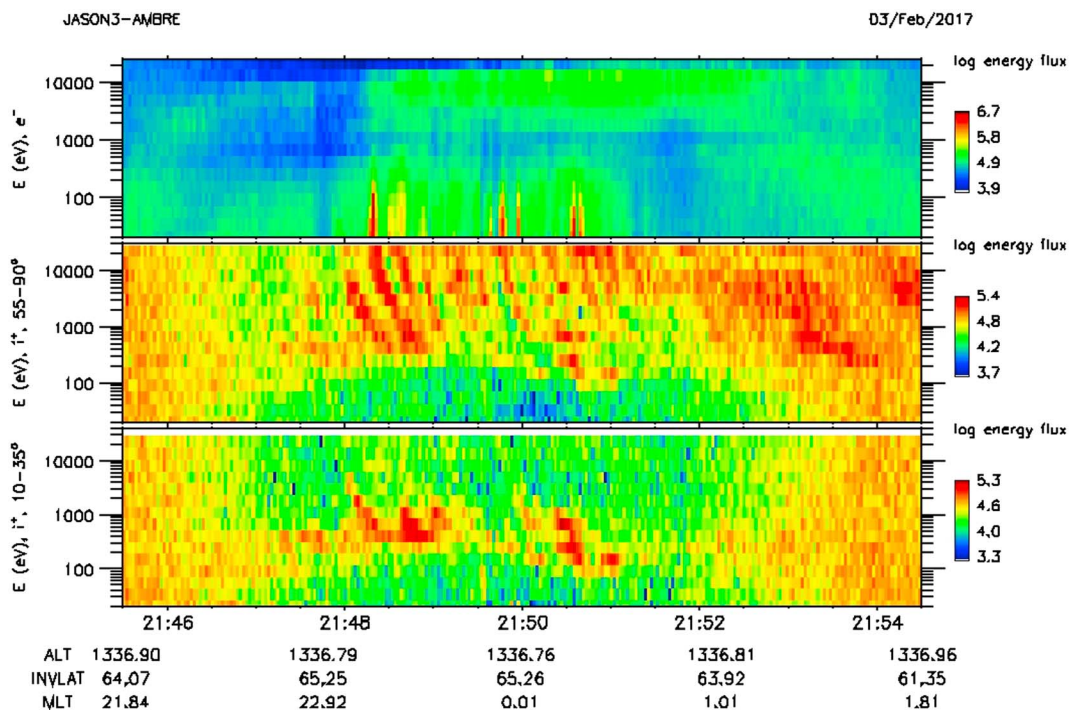


Figure 2. Color-coded particle spectrograms for the 3 February 2017 pass: (top) electrons from 20 eV to 28 keV measured over 180°, (middle) ions from 20 eV to 28 keV at pitch angles between 55° and 90°, and (bottom) ions at pitch angles between 10° and 35°.

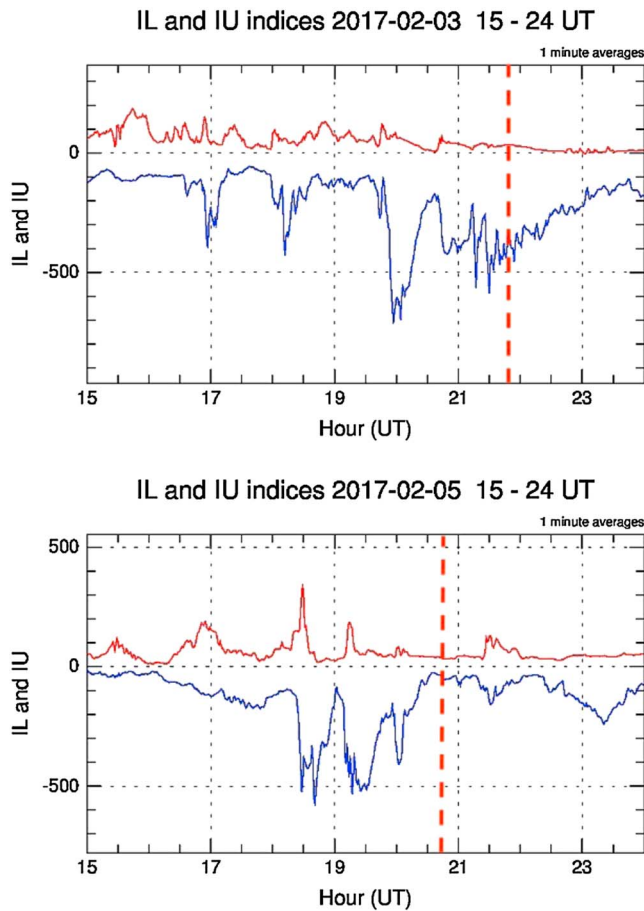


Figure 3. (a) IL (AL) and IU (AU) indices for the 3 February 2017 pass. (b) Identical to (a) but for the 5 February 2017 pass.

pronounced in the spectrogram of 10–35° pitch angle ions (bottom panel). This is a quite general trend of the dispersion features reported in this study, indicative of a prominent flux anisotropy in the 2–10 keV energy range. The dispersion of precipitating ions resembles that of trapped ions but spreads over a smaller energy range. In both cases, a low-energy cutoff is noticeable at 200–300 eV.

Figure 4 provides another example of ion structures occurring two days later on 5 February 2017 during the recovery phase ($Dst = -18$ nT in Figure 1) of the same small storm. IL and IU variations for this latter case are shown in Figure 3b. This JASON-3 pass occurs during a quiet period that immediately follows some severe substorms with IL reaching -500 nT. In Figure 4, the electron spectrogram (top panel) clearly shows the outer radiation belt background as well as a two-component auroral precipitation, one of these components reaching 10 keV while the other is less energetic and extends from a few tens of eV up to ~ 5 keV. The equatorward boundary of the diffuse auroral zone is here encountered near 20:36 UT. The ion spectrograms in Figure 4 again display microinjections with a maximum duration of ~ 25 s, some of these structures being embedded within the outer radiation belt on the ascending part of the orbit. As in Figure 2, the nearly field-aligned ions (with pitch angles between 10° and 35°; bottom panel of Figure 4) exhibit much less clear structures with the exception of one that begins at 20:40:30 UT and lasts about 20 s. This isolated structure is associated with another remarkable one in the trapped ion spectrogram (center panel). A main difference between Figures 2 and 4 is that in the latter figure, there is no evidence of discrete auroral electron structures associated with the ion bands.

In both Figures 2 and 4, it can be seen that microinjections begin at 28 keV, which is the AMBRE highest energy channel so that these structures very likely extend above this upper threshold. This suggests that the ions involved in the observed structures could be protons since CRRES observa-

tions revealed that these ions may account for up to 60–90% of the total ion density in the 20–426 keV range at $L \approx 5$ during disturbed times (e.g., Daglis et al., 1995) and the low-energy component contributes most to the density. Moreover, a statistical analysis of Cluster ion data between 1 and 40 keV/q indicates that the mean proton density in the 7–8 L range always exceeds the O^+ density by a factor 5 ($Kp = 4$) or even 7 ($Kp = 2$) (Maggiolo & Kistler, 2014).

Figure 5 provides three other examples of successive ion microinjections before and after midnight. These passes occur on 9 and 16 September 2017 and on 15 October 2017 during the recovery phase of three storm onsets occurring on 7 September, 14 September, and 11 October 2017 (see Figure 1). At the time of the measurements, Dst values were -92 nT and -32 nT and -40 nT, respectively. In Figure 5, the 180° electron spectrogram and the nearly trapped ion spectrogram are plotted for each case. In the two September cases, dispersed ion structures are detected without any counterpart in the electron spectrogram, while for the October case, weak discrete electron structures can at times be seen in conjunction with the ion structures. Note here that these microinjections are detected at somewhat lower invariant latitudes than in the preceding examples displayed in Figures 2 and 4 (viz., between 62° and 64° on 9 September 2017, between 61.5° and 62° on 16 September 2017, and between 58° and 62° on 15 October 2017). As in the preceding cases, the ion structures are much fainter (or even vanish) in the nearly parallel direction (not shown). Altogether, Figures 2, 4, and 5 demonstrate that JASON-3 frequently encounters quasiperiodic ion microinjections inside the diffuse auroral zone during the recovery phase of storms. The cases presented above demonstrate that the observed microinjections start close to the equatorward boundary of the diffuse auroral zone. However, in a few cases, JASON-3 encountered them in various regions of the diffuse auroral zone, from the southward boundary of the discrete oval down to the outer radiation belt.

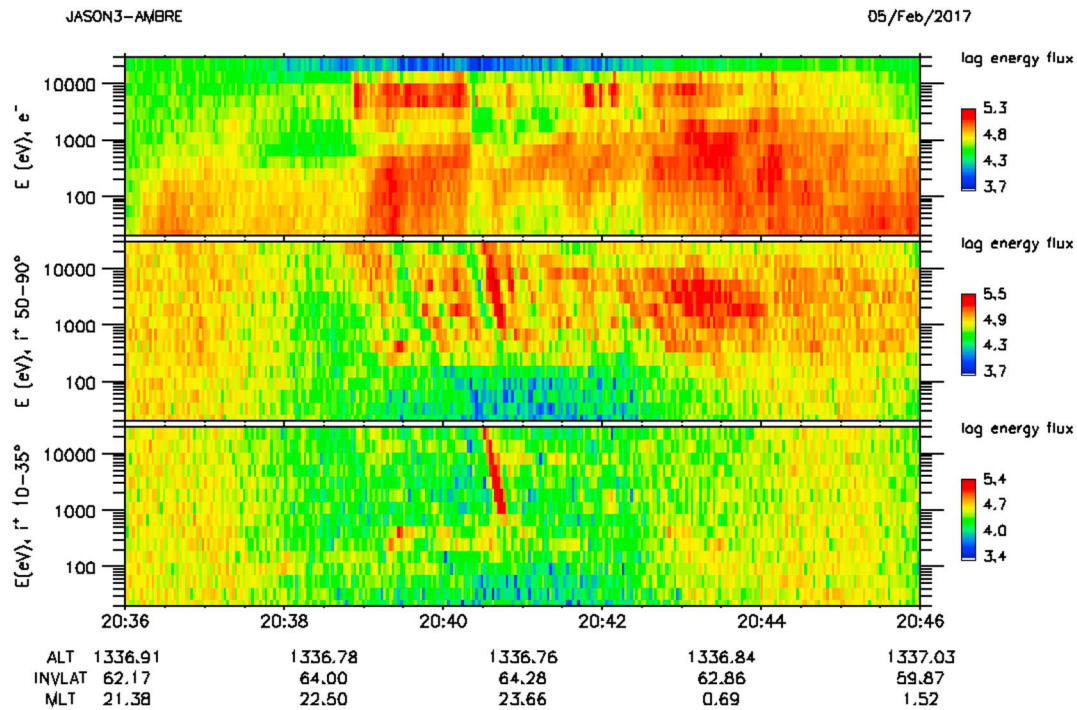


Figure 4. Identical to Figure 2 but for the 5 February 2017 pass.

4. Possible Origin of the Ion Energy Microinjections

To our knowledge, the ion structures presented above with dispersed ions that propagate downward near the equatorward edge of the auroral zone have not been reported so far in the literature. For instance, in the FREJA observations of Hultqvist (2002), downward acceleration of ions (up to 3 keV) was reported at auroral latitudes but velocity dispersion effects were not considered of importance. The features described in the present study are characterized by small time scales (typically, 10 to 20 s), which leads us to refer to them as “microinjections.” It is unlikely that the ions involved in these features originate from the magnetospheric equatorial region since the one-fourth bounce difference between 20 and 1 keV ions reaches more than 60 s at $L = 5$ and thus largely exceeds a single injection duration. A simple way to evaluate the altitude of generation of these ions is to check if the ion structures vary linearly while plotting $1/V$ as a function of time. Such a fit is presented in Figure 6 for a selection of energy bands. It is apparent that the observed structures can be reasonably well approximated by straight lines, yielding an injection distance from JASON-3 of $\sim 1.2 R_E$. At this distance, ions likely are accelerated by some process and they subsequently propagate downward, reaching the spacecraft at distinct times depending upon their energy, hence, the observed dispersions. This linear relationship holds for all the microinjections reported here, provided that they are clear enough to allow a fit.

To take into account pitch angle variations along the particle paths as they approach the ionosphere, single particle tracing backward in time from JASON-3 position was performed using Tsyganenko (1989) magnetic field model (with Kp level of 2 for the selected observation periods). Two examples of trajectory computations are shown in Figure 7, considering distinct initial positions within the ion structures of 3 and 5 February 2017 (shown in blue and red, respectively). It can be seen in this figure that for nearly field-aligned ions (i.e., 25° at JASON-3 altitude; trajectories shown in red), the ion paths converge near 8,100 km altitude (the local pitch angle being of $\sim 8^\circ$), while for trapped ions (i.e., 80° at JASON-3 altitude; trajectories shown in blue), ion path convergence occurs above 10,000 km altitude (local pitch angle of 15°).

These calculations provide insights into the altitudinal region where microinjections are produced but the question remains on the mechanism responsible for the production of such structures. In this regard, it is not possible to thoroughly explore the physical process responsible for the observed injections using JASON-3 data since AMBRE is the only instrument that measures plasma parameters. Several mechanisms can be considered that invoke either direct wave-particle interactions and/or scattering by an impulsive

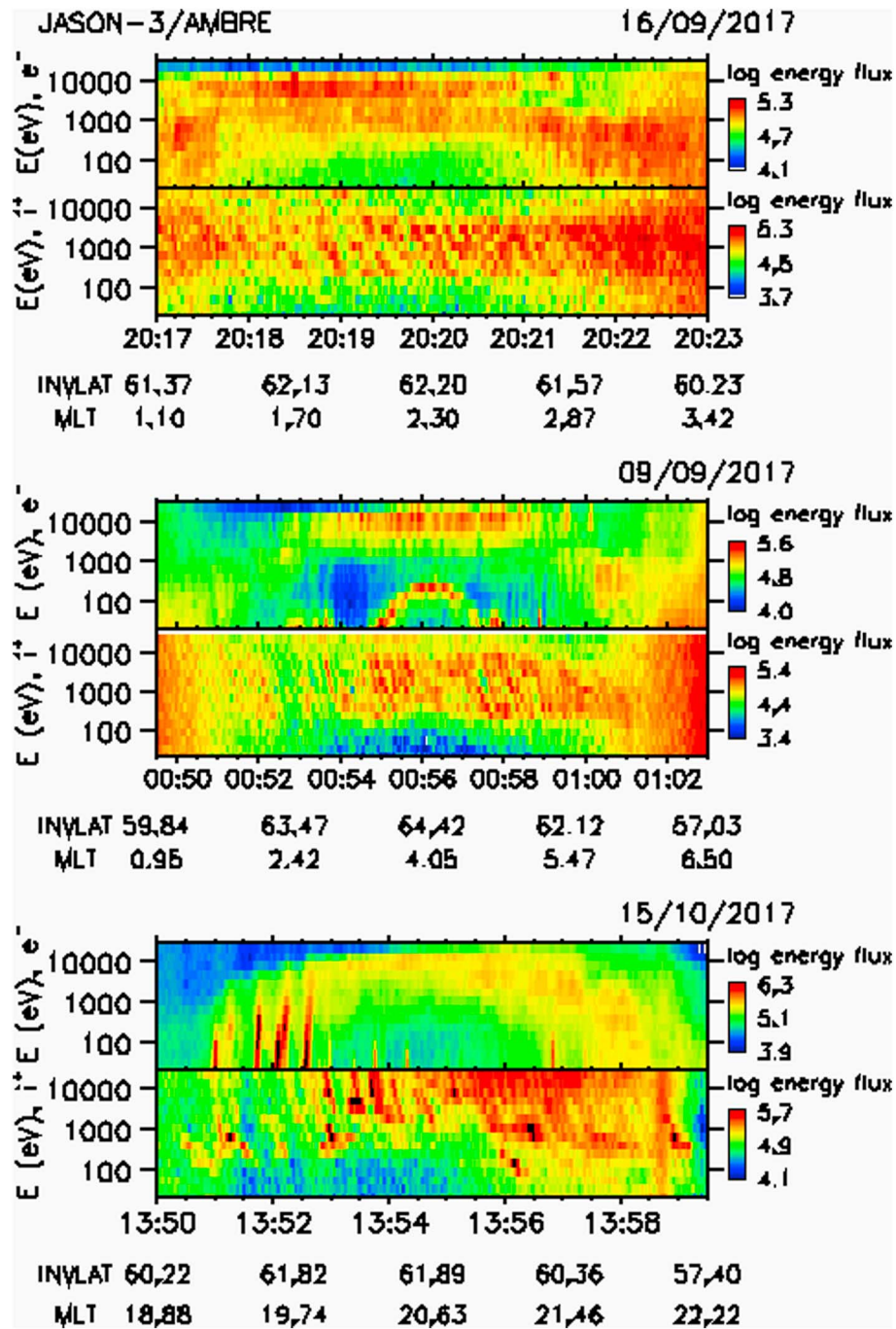


Figure 5. Color-coded energy flux for electrons measured over 180° and ions with pitch angles between 55° and 90° for passes occurring on (top) 16 September 2017, (middle) 9 September 2017, and (bottom) 15 October 2017 (see Figure 1).

electric field. Here it should be stressed that the generation process must be short-lived and recurrent. This excludes the possibility of a static electric field that would smear out the energy dispersions. After the occurrence of a microinjection, another one of these acceleration structures must develop to produce the subsequent microinjection that is observed by JASON-3 as it flies in longitude/latitude. In other words, the very recurrence of the banded pattern recorded along JASON-3 pass contains information on the physical mechanism at work at higher altitudes, although its exact nature cannot be determined from the AMBRE data alone.

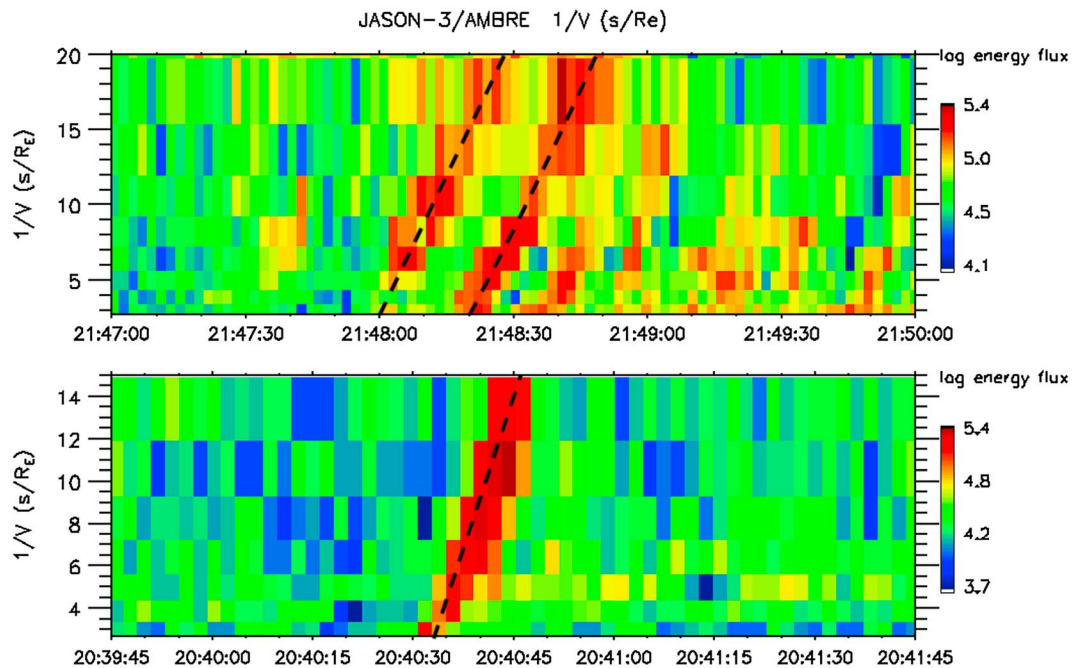


Figure 6. $1/V$ versus time spectrograms for two events occurring on (top) 3 February 2017 and (bottom) 5 February 2017. For propagation dispersion of the ions, this should be a linear relationship, with the slope determining the distance to the source location.

Various studies have shown that EMIC and fast magnetosonic waves can resonate with protons and favor their precipitation via scattering toward the loss cone (e.g., Jordanova et al., 2007; Xiao et al., 2014). However, linear calculations of the diffusion coefficients that require detailed knowledge of the amplitudes and spectral properties of the waves generally consider bounce-averaged conditions and lead to interaction times of at least 1 min to efficiently scatter protons. These processes can be at the root of the presence of the ion reservoir at altitudes higher than about 10,000 km but cannot explain the formation of microinjections toward low altitudes. In order to explain the present observations, the source process must be located out-

side the equator and acting over a time scale of at most several seconds. Nonlinear interactions, which prevail off-equator where particles have an increasing perpendicular velocity and where waves have an increasing perpendicular component of the normal vector, occur on such small time scales (e.g., Zhu et al., 2012) and thus appear as good candidates to explain the observations.

As demonstrated in Figures 4 and 5, ion microinjections may be either associated with discrete electron structures or not. To better demonstrate this phenomenon, we searched for additional cases where the ion dispersions can be related without any ambiguity with discrete auroral structures embedded in the diffuse auroral zone (i.e., in conjunction with an adjacent enhanced upward current). Figure 8 presents an example on 27 October 2016 in the evening sector during a storm recovery period. In this case, more accurate particle energy spectra (viz., 32 energy steps in 1 s) were acquired with the AMBRE instrument. It is clearly apparent from Figure 8 that some ion dispersions are closely related with electron structures. Here again, the maximum energy of the ion dispersions reaches the upper limit (28 keV) of the detector so that the downflowing population likely extends above this limit. For this case, the microinjections are nearly periodic with a period of about 15 s. More generally, all observed microinjections exhibit some quasiperiodicity with a recurrence time

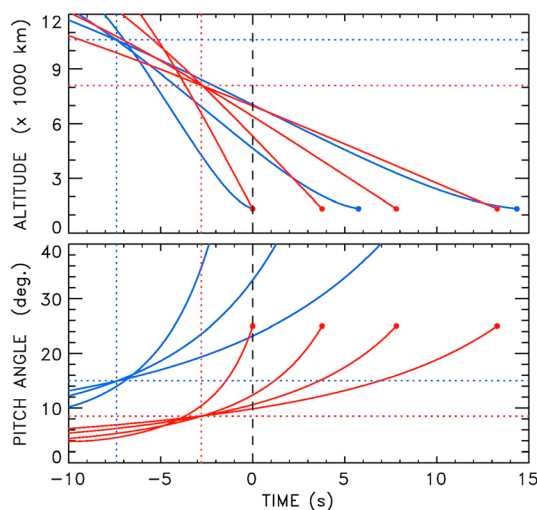


Figure 7. Particle tracing backward in time from JASON-3 position for two ion microinjections: (top) altitude and (bottom) pitch angle versus time. The blue and red trajectories correspond to ions that are trapped (80° pitch angle) and nearly field-aligned (25° pitch angle) at JASON-3 altitude, respectively. The time $t = 0$ corresponds to the detection time of the highest energy ions.

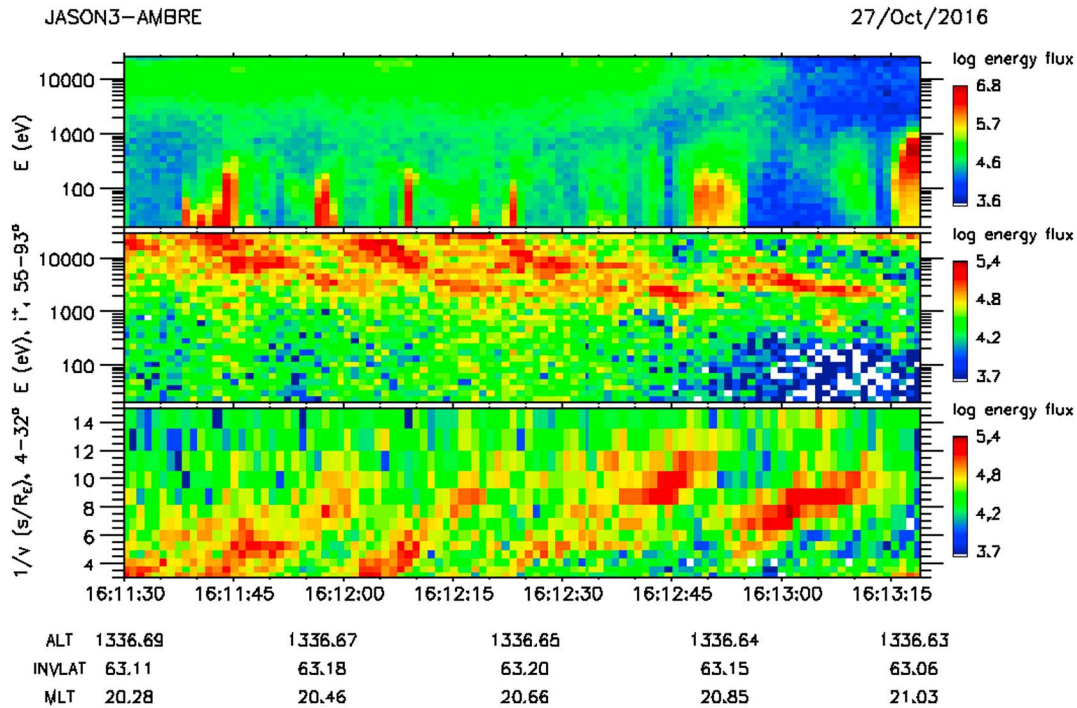


Figure 8. Color-coded particle spectrograms: (top) electrons from 20 eV to 28 keV measured over 180°, (middle) ions from 20 eV to 28 keV at pitch angles between 55° and 93°, and (bottom) 1/V versus time spectrogram of ions with pitch angles between 4° and 32°.

varying from 10 up to 25 s. This recurrence time scale of microinjections is reminiscent of ground Pi1-ULF pulsations, which consist of magnetic pulses spaced irregularly 1–40 s apart (Heacock, 1967). To check this hypothesis, we performed a search of pulsations using conjugate rapid-run magnetometers in Scandinavia. Figure 9 presents such magnetic field and ion data for the 9 March 2017 event. The satellite was flying over

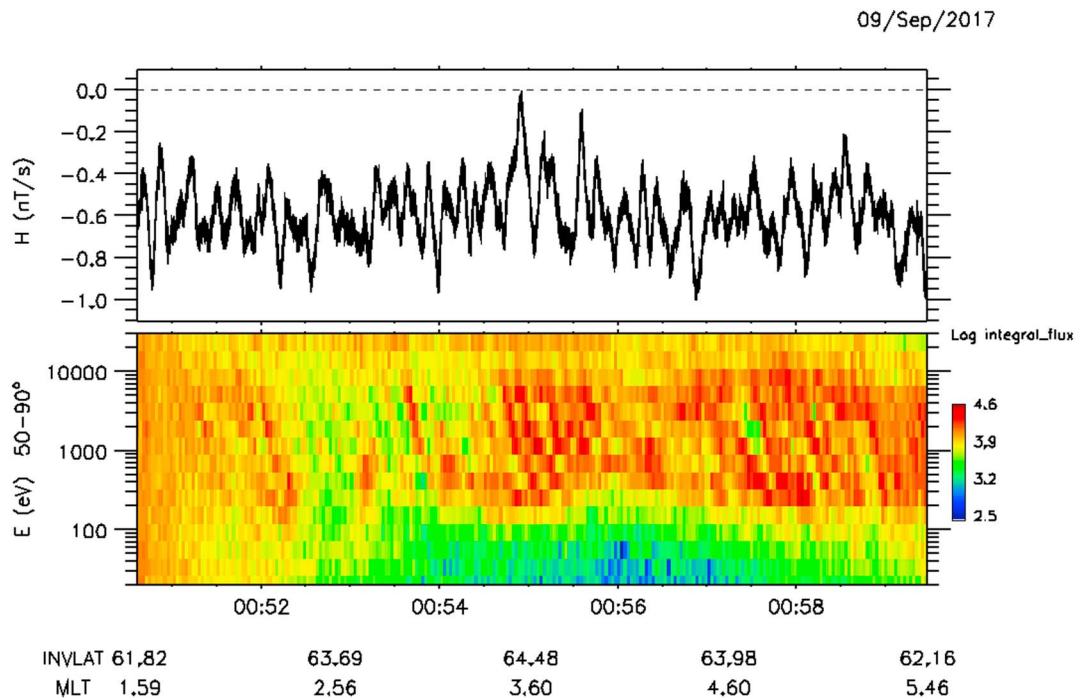


Figure 9. Comparison of the pulsation magnetometer H component at Rovaniemi and recurrent microinjections measured on 9 September 2017. The Finnish Rovaniemi ground station is located inside the spacecraft conjugate area.

the Finnish Rovaniemi station located at 63.6° invariant latitude close to the JASON-3 field line foot when recurrent microinjections were detected. The top of Figure 9 presents the corresponding pulsation magnetometer H component. The bottom panel shows the ion data in the 50° – 90° pitch angle range. There is a clear relationship between the ion and magnetic Pi1 pulsations with a 10 s quasiperiodicity (with a superimposed high-frequency signal, between 3 and 10 Hz). Two other microinjection events associated with micropulsation were detected on 3 and 5 February 2017 (see also Figures 2 and 4). These ion injections occurred again in association with Pi1 magnetic pulsations (not shown) with superimposed higher frequency signals between about 3 and 10 Hz. As shown by Arnoldy et al. (1992), Pi1 originate from local ionospheric currents, magnetospheric waves, and resonant cavity modes.

This relationship between magnetic pulsations and microinjections leads us to propose that the injections could be due to nonlinear interaction of ions with EMIC waves whose amplitude is being modulated by ULF waves, as shown, for example, by Rasinkangas and Mursala (1998) and Usanova et al. (2010).

5. Conclusions

During weak and moderate magnetic storms, the AMBRE experiment onboard JASON-3 repeatedly recorded recurrent dispersed ion structures on the equatorward side of the diffuse auroral zone, some of them in association with embedded small arcs. Because they occur on time scales of a few seconds, we refer to these structures of downflowing time-of-flight dispersed ion structures as microinjection features, which to our knowledge have not been reported so far in this region of space. Ray tracing of these injections suggests that the particles propagate downward from a source located not in the equatorial region but at altitudes between 8,000 and 11,000 km, with an upper limit near $2.2 R_E$. In some instances, up to 10 structures have been recorded in the 200 eV–28 keV energy range at invariant latitudes between 61° and 65° (equivalently, L parameter between 4.25 and 5.4). During such disturbed periods, the equatorward boundary of the diffuse auroral zone is close to (or even adjacent to) the plasmopause and the ion ionospheric trough (Moldwin et al., 2002; Yizengaw et al., 2005). A possible mechanism at the root of such dispersions is the acceleration and angular scattering following nonlinear interaction of ions with EMIC waves at midaltitudes. The close association of microinjection recurrence with Pi1 waves recorded close to the conjugate footprint of the spacecraft suggests a causal relationship between microinjection recurrence and magnetic pulsations, which could modulate EMIC waves. Still, thorough investigation of the mechanism responsible for these ion structures and for the associated electron structures, which appears as an important element of the overall auroral electrodynamics, clearly requests further studies and awaits a spacecraft with instrumentation fully dedicated to auroral physics.

Acknowledgments

The AMBRE instrument onboard the French-U.S. JASON-3 spacecraft has been constructed under CNES leadership by EREMS and COMAT. IRAP has provided the general design of the analyzers, of the MCP stacks and HVs. Data are received at CNES and formatted at ONERA/DEPhIEE, Toulouse. IRAP provides the data treatment and scientific analysis. We are grateful to E. Penou, who developed the software project clweb (<http://clweb.irap.omp.eu>) that is used in the present analysis. Dst index comes from the WDC-2, Kyoto. The International Monitor for Auroral Geomagnetic Effects (IMAGE) has provided the IL and IU indices. The authors thank the referee who drew their attention to the wave nature of microinjections

References

- Arnoldy, R. L., Posch, J. L., Engebretson, M. J., Fukunishi, H., & Singer, H. J. (1992). Pi1 magnetic pulsations in space and at high latitudes on the ground. *Journal of Geophysical Research*, *103*, 23,581–23,591. <https://doi.org/10.1029/98JA01917>
- Boehm, M., Klumppar, H., Möbius, D. M., Kistler, E. L., McFadden, J. P., Carlson, C. W., & Ergun, E. E. (1999). Fast auroral snapshot observations of bouncing ion distributions—Field line length measurements. *Journal of Geophysical Research*, *104*, 2343–2355. <https://doi.org/10.1029/98JA02290>
- Colpitts, C. A., Catell, C. A., Kozyra, J. U., & Parrot, M. (2012). Satellite observations of banded VLF emissions in conjunction with energy-banded ions during very large geomagnetic storms. *Journal of Geophysical Research*, *117*, A10211. <https://doi.org/10.1029/2011JA017329>
- Daglis, Y. A., Axford, W. I., Livi, S., Wilken, B., Grande, M., & Söraas, F. (1995). Auroral ionospheric ion feeding of the inner plasma sheet during substorms. *Journal of Geomagnetism and Geoelectricity*, *48*, 729–739. <https://doi.org/10.5636/jgg.48.729>
- Delcourt, D. C., Dubouloz, N., Sauvaud, J.-A., & Malingre, M. (1999). On the origin of sporadic keV ion injections observed by Interball-Auroral during the expansion phase of a substorm. *Journal of Geophysical Research*, *104*, 24,929–24,937. <https://doi.org/10.1029/1999JA900302>
- Frahm, R. A., Reiff, P. H., Winningham, J. D., & Burch, J. L. (1986). Banded ion morphology: Main and recovery phases. In T. Chang (Ed.), *Ion Acceleration in the Magnetosphere and Ionosphere*, *Geophysical Monograph Series* (Vol. 38, p. 98). Washington, DC: American Geophysical Union.
- Heacock, R. R. (1967). Two subtypes of Pi micropulsations. *Journal of Geophysical Research*, *72*, 3905–3917. <https://doi.org/10.1029/JZ072i015p03905>
- Hirahara, M., Mukai, T., Nagai, T., Kaya, N., Hayakawa, H., & Fukunishi, H. (1996). Two types of ion energy dispersions observed in the nightside auroral regions during geomagnetically disturbed periods. *Journal of Geophysical Research*, *101*, 7749–7767. <https://doi.org/10.1029/95JA03206>
- Hirahara, M., Yamazaki, A., Seki, K., Mukai, T., Sagawa, E., Kaya, N., & Hayakawa, H. (1997). Characteristics of downward flowing ion energy dispersions observed in the low-altitude central plasma sheet by Akebono and DMSP. *Journal of Geophysical Research*, *102*, 4821–4839. <https://doi.org/10.1029/96JA03332>
- Hultqvist, B. (2002). Downward ion acceleration at auroral latitudes: Cause of parallel electric field. *Annales Geophysicae*, *20*(8), 1117–1136. <https://doi.org/10.5194/angeo-20-1117-2002>

- Jordanova, V. K., Spasojevic, M., & Thomsen, M. F. (2007). Modeling the electromagnetic ion cyclotron wave-induced formation of detached subauroral proton arcs. *Journal of Geophysical Research*, *112*, A08209. <https://doi.org/10.1029/2006JA012215>
- Kovrazhkin, R. A., Sauvaud, J.-A., & Delcourt, D. C. (1999). INTERBALL-Auroral observations of 0.1–12 keV ion gaps in the diffuse auroral zone. *Annales Geophysicae*, *17*(6), 734–742. <https://doi.org/10.1007/s00585-999-0734-9>
- Lui, A. T. Y., Akasofu, S. I., Venkatesan, D., Anger, C. D., Heikkila, W. J., Winningham, J. D., & Burrows, J. T. (1977). Simultaneous observations of particle precipitations and auroral emissions by the ISIS-2 satellite in the 19–24 MLT sector. *Journal of Geophysical Research*, *82*, 2210–2226. <https://doi.org/10.1029/JA082i016p02210>
- Maggiolo, R., & Kistler, L. M. (2014). Spatial variation in the plasma sheet composition: Dependence on geomagnetic and solar activity. *Journal of Geophysical Research*, *119*, 2836–2857. <https://doi.org/10.1002/2013JA019517>
- Mauk, B. H. (1986). Quantitative modeling of the “convection surge” mechanism of ion acceleration. *Journal of Geophysical Research*, *91*, 13,423–13,431. <https://doi.org/10.1029/JA091iA12P13423>
- Moldwin, M. B., Downward, L., Rassoul, H. K., Amin, R., & Anderson, R. R. (2002). A new model of the location of the plasmopause: CRRES results. *Journal of Geophysical Research*, *107*(A11), 1339. <https://doi.org/10.1029/2001JA009211>
- Rasinkangas, R., & Mursala, K. (1998). Modulation of magnetospheric EMIC waves by pc-3 pulsations of upstream origin. *Geophysical Research Letters*, *25*, 869–872. <https://doi.org/10.1029/98GL50415>
- Reiff, P. H., Hill, T. W., & Burch, J. L. (1977). Solar wind plasma injection at the dayside magnetospheric cusp. *Journal of Geophysical Research*, *82*, 479–491. <https://doi.org/10.1029/JA082i004p00479>
- Rosenbauer, H. (1975). HEOS 2 plasma observations in the distant polar magnetosphere: The plasma mantle. *Journal of Geophysical Research*, *80*, 2723–2737. <https://doi.org/10.1029/JA080i019p02723>
- Sauvaud, J. A., Crasnier, J., Mouala, K., Kovrazhkin, R. A., & Jorjio, N. V. (1981). Morning sector ion precipitation following substorm injections. *Journal of Geophysical Research*, *86*, 3430–3438. <https://doi.org/10.1029/JA086iA05p03430>
- Sauvaud, J.-A., & Payan, D. (2017). Résultats préliminaires de l'expérience de mesure des particules AMBRE installée à bord du satellite JASON-3, CNES report, Toulouse, DSO/TB/EL/2017–15526.
- Sauvaud, J.-A., Popescu, D., Delcourt, D. C., Parks, G. K., Brittnacher, M., Sergeev, V., et al. (1999). Sporadic plasma sheet ion injections into the high altitude auroral bulge—Satellite observations. *Journal of Geophysical Research*, *104*, 28,565–28,586. <https://doi.org/10.1029/1999JA900293>
- Sergeev, V. A., Sauvaud, J.-A., Popescu, D., Kovrazhkin, R. A., Lutsenko, V. N., Zelenyi, L. M., et al. (2000). Plasma sheet ion injections into the auroral bulge: Correlative study of spacecraft and ground observations. *Journal of Geophysical Research*, *105*, 18,465–18,481. <https://doi.org/10.1029/1999JA900435>
- Shelley, E. G., Sharp, R. D., & Johnson, R. G. (1976). He⁺⁺ and H⁺ flux measurements in the dayside cusp: Estimates of convection electric field. *Journal of Geophysical Research*, *81*, 2363–2370. <https://doi.org/10.1029/JA081i013p02363>
- Smith, M. F., & Lockwood, M. (1996). Earth's magnetospheric cusps. *Reviews of Geophysics*, *34*, 233–260. <https://doi.org/10.1029/96RG0089>
- Stenuit, H., Sauvaud, J.-A., Delcourt, D. C., Mukai, T., Kokubun, S., Fujimoto, M., et al. (2001). A study of ion injections at the dawn and dusk polar edges of the auroral oval. *Journal of Geophysical Research*, *106*, 29,619–29,631. <https://doi.org/10.1029/2001JA900060>
- Tsyganenko, N. A. (1989). Magnetospheric magnetic field model with a warped tail current sheet. *Planetary and Space Science*, *37*(1), 5–20. [https://doi.org/10.1016/0032-0633\(89\)90066-4](https://doi.org/10.1016/0032-0633(89)90066-4)
- Usanova, M. E., Mann, I. R., Kale, Z. C., Rae, I. J., Zydora, R. D., Sandanger, M., et al. (2010). Conjugate ground and multisatellite observations of compression related EMIC pc-1 waves and associated proton precipitation. *Journal of Geophysical Research*, *115*, A07208. <https://doi.org/10.1029/2009JA014935>
- Winningham, J. D., Burch, J. L., & Frahm, R. A. (1984). Bands of ions and angular V's: A conjugate manifestation of ionospheric ion acceleration. *Journal of Geophysical Research*, *89*, 1749–1754. <https://doi.org/10.1029/JA089iA03p01749>
- Woch, J., & Lundin, R. (1992). Signatures of transient boundary layer processes observed with Viking. *Journal of Geophysical Research*, *97*, 1431–1447. <https://doi.org/10.1029/91JA02490>
- Xiao, F., Zong, Q., Wang, Y., He, Z., Su, Z., Yang, C., & Zhou, Q. (2014). Generation of proton aurora by magnetosonic waves. *Scientific Reports*, *4*(1). <https://doi.org/10.1038/srep05190>
- Yamauchi, M., Ebihara, Y., Nilsson, H., & Dandouras, I. (2014). Ion drift simulation of sudden appearance of sub-keV structured ions in the inner magnetosphere. *Annales Geophysicae*, *32*(2), 83–90. <https://doi.org/10.5194/angeo-32-83-2014>
- Yizengaw, E., Wei, H., Moldwin, M. B., Galvan, D., Mandrake, L., Mannucci, A., & Pi, X. (2005). The correlation between mid-latitude trough and the plasmopause. *Geophysical Research Letters*, *32*, L10102. <https://doi.org/10.1029/2005GL022954>
- Zhu, H., Su, Z., Xiao, F., Zheng, H., Shen, C., Wang, Y., & Wang, S. (2012). Nonlinear interaction between ring current protons and electromagnetic ion cyclotron waves. *Journal of Geophysical Research*, *117*, A12217. <https://doi.org/10.1029/2012JA018088>